Chapter 10

Beam Transport Lines and Injection System

10.1 Beam Transport Lines

The beam parameters of the beam transport lines for SuperKEKB and KEKB are shown in Table 10.1. The most significant difference from the KEKB is that the energy of the positron line increases to 4 GeV from 3.5 GeV. Almost all components of the beam transfer lines, which convey electrons and positrons to the HER and LER of KEKB, are planned to be reused for the corresponding beam lines in the SuperKEKB . Several modifications in the positron line are required in accordance with the energy change:

- Reconstruction of the ECS layout in the SY3.
- The BH2P-type and BH3P-type bends are modified in the air gap to increase the magnetic field without changing current.
- Maximum current of the power supplies is increased for bends B3P, BH1CP, BH1P, and BV2P.

For both lines sextupole magnets are installed in the dispersive section in order to correct high-order dispersion, Because of low emittance it emerges

Table 10.1: Beam parameters in comparison with the KEKB

	SuperKEKB		KEKB		unit
	e-	e+	e-	e+	
Beam energy	7	4	8	3.5	GeV
Emittance	$1.46^{\dagger 1}$ / $4.77^{\dagger 2}$	12.8	23	200	nm
Energy spread	0.1	0.125	0.125	0.125	%
Charge/bunch	4	4	1	0.5	nC
No. of bunch/pulse		2			
Rep. rate		50			Hz

†1 at the end of Linac. †2 at the end of the beam line.

as one of major sources of the emittance degradation.

10.1.1 Changes in the layout of ECS in the SY3

The ECS system for the positron beam is composed of a chicane and two S-band accelerating structures. Since the design energy is changed from 3.5 GeV to 4.0 GeV magnetic field of bends that are used to make the chicane orbit also has to be increased by a ratio of 4/3.5=1.143 in order to obtain the same R_{56} component. Because the first bend BC1P.1, which has a very wide poles, is not accessible with a crane it is difficult as well as expensive to replace with a new magnet. We have adopted another option: we use the BC1P with the magnetic field unchanged while the other four bends are replaced with new magnets. The last bend BC1P.2 is also reused for symmetry. Figure 10.1 shows layout of ECS in the SY3. Accelerating structures ACC.1 and ACC.2 are moved to downstream while preserving the position of B1P. Specifications of ECS bends are shown in the Table 10.2. Since the energy of electrons is decreased from 8 GeV to 7 GeV the bend angle of BC1P.1 for electrons get larger. To preserve the positions of magnets at downstream of B0E the increased angle is compensated by exciting BHD0.1, which has been set zero

in the KEKB and energized only in the operation of the beam-dump mode.

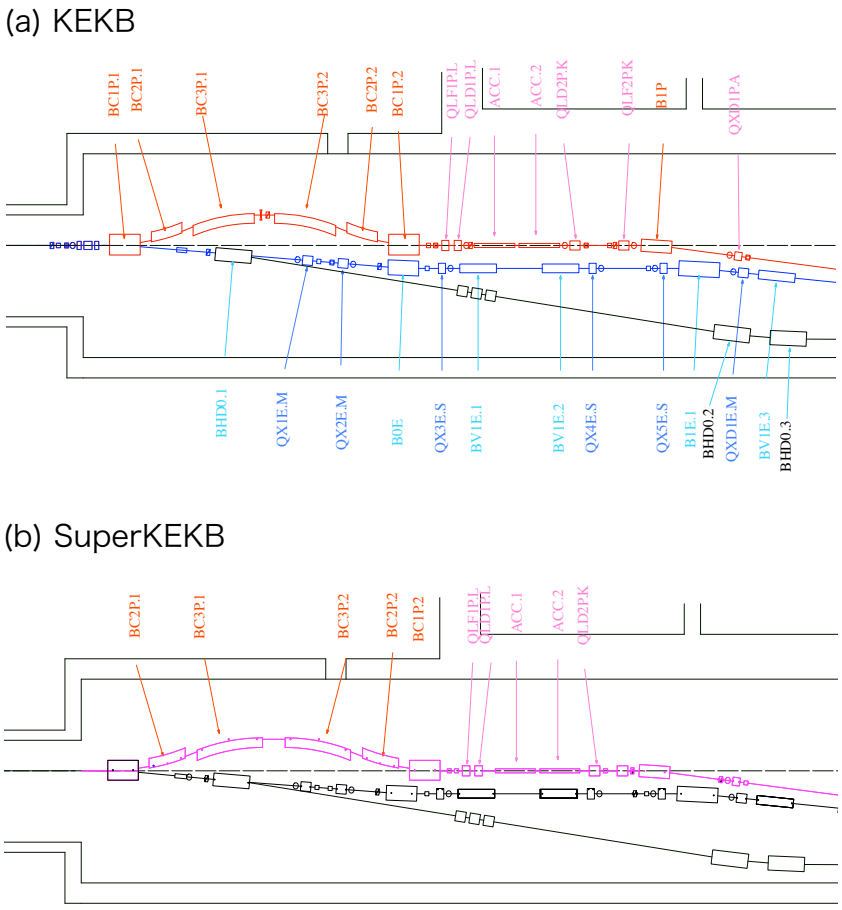

Figure 10.1: Layout of the ECS in the SY3. (a) for the old KEKB, (b) for the SuperKEKB

10.1.2 Changes of the magnet system in the positron line

Magnets of the positron line are classified into four categories according to its degree of modification in application to the upgraded beam line: (A)

Table 10.2: Specifications of ECS bends

	BC1P	BC2P	BC3P	unit
Bend angle	.1648	.2116	-.3764	rad
Magnetic field	1.427	1.501	1.510	T
Air gap	25	20	20	mm
Pole width	320	150	150	mm
Core length	1.0	1.771	3.210	m

both the aperture and the maximum current of the power supply must be upgraded, (B) the aperture must be modified while the power supply can be used without modification, (C) the aperture need not be changed but the power supply must be upgraded, (D) usable without any changes. No magnet, fortunately, falls to A. All quadrupoles, steering magnets, and roughly half of the bends go to category D, while rest of bends falls under B or C:

(B) Seven BH2P-type bends and eleven BH3P-type bends used in the Arc-2 and Arc-3, respectively, are modified in there aperture from 40 mm to 34 mm by inserting a flat silicon-steel plate with thickness of 6 mm between the pole-block and the return yoke. A simulation of the magnetic field shows no significant degradation in the field profile.

(C) Maximum current of the power supplies for bends B3P, BH1CP, BH1P, and BV2P is increased. Maximum voltage of these power supplies need not be upgraded because the regulator voltage has enough margin.

10.1.3 Stability of power supplies

Since the beam emittance from the Linac is very small, about 4 % of that in KEKB, stability of power supplies, which is expected to be reused, might be a concern. If deviations from the design values (errors) is static, they can be corrected with ordinary orbit/optics correction technique using orbit/wire

measurements. For an error that varies with higher frequency, it will produce an orbit jitter or a jitter in beta-functions at the injection point, depending on whether the error be dipole or quadrupole.

First, in the quadrupole case, jitter in beta-functions generates larger effective-emittance. It can be quantified by so called *Beta mismatch* B_m,

$$B_m = \frac{1}{2}\left(\frac{\beta^*}{\beta} + \frac{\beta}{\beta^*}\right) + \frac{1}{2}\left(\alpha^*\sqrt{\frac{\beta}{\beta^*}} - \alpha\sqrt{\frac{\beta^*}{\beta}}\right)^2 , \tag{10.1}$$

where, α^* and β^* are changed values of α and β due to quadrupole errors. The beta-mismatch due to a single quadrupole error Δk_j in the beam line is calculated from Eq. (10.1), assuming the thin lens model, as $\Delta B_m = 1 + (\beta_j \Delta k_j)^2/2$, where β_j is the beta-function at the error source. Taking summation over all the quadrupoles we obtain the beta-mismatch at the end of the beam line,

$$B_m = \prod_j \left[1 + (\beta_j \Delta k_j)^2/2\right] \simeq 1 + \sum_j (\beta_j \Delta k_j)^2/2 \,, \tag{10.2}$$

where we assumed no correlation exists between errors. In correlated case the beta-mismatch would be less than Eq. (10.2). The second term can be estimated using $\sum_j (\beta_j k_j)^2/2 = 2405$, $\sum_j (\beta_j k_j)^2/2 = 2770$ for horizontal and vertical plane of the positron line, respectively. Assuming $\Delta k_j/k_j = 5 \times 10^{-4}$ the effective emittance increases by a negligible amount, $\Delta\epsilon/\epsilon = B_m - 1 = 6 \times 10^{-4}$, and 6.9×10^{-4}. The similar estimation holds for the electron line.

Secondly we investigate the effect of a random dipole kick on the effective emittance due to a strength error of power supplies for bending magnets. The beam ellipses overlaid in the phase space, with its centroid randomly shifted by pulse to pulse, would have larger emittance compared to that of a single bunch. Denoting the centroid shift (X, X'), sizes of the overlaid beam can be expressed by

$$\hat{\beta}\hat{\epsilon} \equiv \left\langle (x+X)^2 \right\rangle = \left\langle x^2 \right\rangle + \left\langle X^2 \right\rangle = \beta\epsilon + \left\langle X^2 \right\rangle , \tag{10.3}$$

$$-\hat{\alpha}\hat{\epsilon} \equiv \langle (x+X)(x'+X') \rangle = \langle xx' \rangle + \langle XX' \rangle = -\alpha\epsilon + \langle XX' \rangle , \tag{10.4}$$

$$\hat{\gamma}\hat{\epsilon} \equiv \left\langle (x'+X')^2 \right\rangle = \left\langle x'^2 \right\rangle + \left\langle X'^2 \right\rangle = \gamma\epsilon + \left\langle X'^2 \right\rangle . \tag{10.5}$$

From Eqs. (10.3)-(10.5) the effective emittance is written as

$$\begin{aligned}\hat{\epsilon^2} &= (\beta\epsilon + \langle X^2\rangle)(\gamma\epsilon + \langle X'^2\rangle) - (-\alpha\epsilon + \langle XX'\rangle)^2 \\ &= \epsilon^2 + \langle X^2\rangle\langle X'^2\rangle - \langle XX'\rangle^2 + \left(\beta\langle X'^2\rangle + 2\alpha\langle XX'\rangle + \gamma\langle X^2\rangle\right) \quad (10.6)\end{aligned}$$

The centroid shift is expressed by a summation of shift due to each error-kick θ_i:

$$X = \sum_i M_{12}(i)\theta_i\,, \quad (10.7)$$

$$X' = \sum_i M_{22}(i)\theta_i\,, \quad (10.8)$$

where $M(i)$ is a transfer matrix from the error source to the observation point. Given the transfer matrix we can estimate the effective emittance under appropriate assumptions on the error kicks. For the electron line, for example, it is evaluated as

$$\hat{\epsilon}_h^2 = \epsilon_h^2 + 117.5\,\delta^4 + 28.5\,\epsilon_h\delta^2\,, \quad (10.9)$$

$$\hat{\epsilon}_v^2 = \epsilon_v^2 - 4\times10^{-7}\,\delta^4 + 0.12\,\epsilon_v\delta^2\,, \quad (10.10)$$

where δ is the current jitter of power supplies. We have assumed $\langle\theta_i\theta_j\rangle = \Theta_i\Theta_j\delta^2$ if i and j belongs to the common power supply, otherwise $\langle\theta_i\theta_j\rangle = 0$, where Θ_i and Θ_j are the design bend-angle of the magnet. In the vertical plane the emittance is insensitive to the current jitter of the power supplies because in almost cases the optics is designed such that the dispersion function is closed at the end of a region subtended by vertical bends that are connected to a common power-supply. Using the measured current-ripple of $\delta = 4.5$ ppm , whose dominant frequency is 300 Hz, and $\epsilon_h = 1.46$ nm, we estimate that $\hat{\epsilon}/\epsilon = 1.2$. Taking into account of an effect of eddy current in the vacuum chamber, which is made of aluminum with thickness of 3 mm, magnetic field in the chamber will be suppressed by an order of magnitude. Thus the effect of the current-ripple on the emittance is expected to be negligibly small. The same conclusion holds for the power supplies of the positron line.

10.1.4 Emittance growth due to synchrotron radiation

The quantum nature of synchrotron radiation induces a transverse emittance. The beam transport lines to the main rings comprise of four major arcs and they have many dipole magnets with the bend-angle surpassing 5 radian in total, which was a consequence of complicated geometry bypassing the PF-AR[2]. Since the emittance growth scales as E^5/ρ^3 and and linearly depends on the total bend angle the higher energy (electron) line is expected to have larger effects. The emittance including the quantum excitation is expressed as the same form as the Eq. (10.6), where X and X' are interpreted as the quantum excitation due to synchrotron radiation at bends. Figure 10.2 shows a simulation results of the horizontal emittance at the end of the electron line as a function of the input emittance, which was obtained with a particle tracking using SAD. The emittance fits well the following equation,

$$\begin{aligned} \epsilon &= \sqrt{\epsilon_0^2 + \epsilon_p \epsilon_0 + \epsilon_q^2} \\ &\text{with} \quad \epsilon_{\rm q} = 2.98 \text{ nm}, \\ &\qquad \epsilon_p = 8.03 \text{ nm}, \end{aligned} \tag{10.11}$$

where, ϵ_0 is the input emittance. For the design emittance of $\epsilon_0 = 1.46$ nm, the actual emittance at the end of beam line increases to 4.77 nm. The beam size at the injection septum is 0.31 mm, assuming $\beta_x = 20$ m. The required injection aperture is still dominated by the septum width of 2.5 mm. Although the emittance growth due to synchrotron radiation is very big, it plays only a minor role on the injection aperture itself. For the vertical plane, the effect of synchrotron radiation on emittance is negligible: $\epsilon_q = 0.0073$ nm, and $\epsilon_p = 0.022$ nm.

10.1.5 Instrumentation

Wire scanners

The wire scanners have been used for the beam size measurement in the beam transport lines from Linac to to the KEKB main rings [1]. The diameter

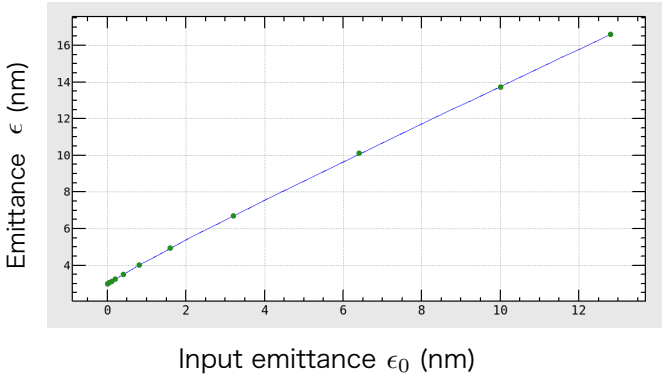

Figure 10.2: Simulation results of the horizontal emittance at the end of the electron line including a synchrotron radiation as a function of input-emittance.

of the wires has been 200 μm, which was sufficiently small compared to the injected beam. In the SuperKEKB, however, the size of the injected beam will be comparable to the wire diameter. In such cases the beam size cannot be measured correctly without corrections of the wire-size effect. Therefore, the wire with a diameter of 60 μm will be used.

10.2 Injection System

In the KEKB [1], the beam injection had been performed with the betatron injection scheme, which inevitably induces betatron oscillation of the injected beam[2]. Since the dynamic aperture of the SuperKEKB is considerably narrower than the KEKB, the injection amplitude has to be much smaller to allow the injected beam stably circulate within the dynamic aperture. It has been pointed out that a transient beam-blowup might occur during injection because of the beam-beam effect[3]. Since the beta-function is strongly

squeezed in the vertical plane at the interaction point, a particle that has a finite vertical amplitude experiences a very strong beam-beam effect during the horizontal oscillation, which is specific in the betatron injection in the nano-beam scheme without using club-waist that has been adopted in the SuperKEKB. To cure the beam loss due to the transient blowup, which depends on the dynamic aperture, we adopt the so called synchrotron injection scheme as a backup option for the injection method. In the synchrotron injection, incoming beam that has an energy offset is injected on the closed orbit with the corresponding energy-offset in the ring, thus inducing no betatron oscillation but in turn the oscillation in the synchrotron phase space. Denoting Δx the distance between the stored beam and the incoming beam, η_R the dispersion function at the injection point of the ring, and δ the energy offset, an equation

$$\Delta x = \eta_R \, \delta$$

has to be satisfied. For the HER we found a design that satisfies above equation. For the LER, however, it is difficult to create the dispersion function at the injection point because of a requirement that the dispersion function at the RF cavities, which are located nearby the injection region, must disappear.

In the SuperKEKB project the old KEKB systems are to be reused as many as possible. Regarding the injection system, half of injection septum magnets that are located near to the main rings are totally reconstructed to make the septum width as thin as possible, thereby reducing the injection amplitude as small as possible. New septum magnets have been designed and constructed based on the careful study of the injection orbit.

10.2.1 Injection Orbit

For the betatron injection, the horizontal dispersion of the ring around the injection region is set to be $\eta_R = 0$; on the other hand, for the synchrotron injection, larger $|\eta_R|$ eases demand for the energy-spread of the incoming

beam. The beam separation Δx between the injected beam and the stored beam is the sum of the effective septum width w_s and the beam size of the two beams:

$$\Delta x = w_s + n_R \sigma_R + n_i \sigma_i \ , \tag{10.12}$$

where n_R and n_i are effective beam sizes of the stored and the injected beam, respectively, in unit of their rms sizes, σ_R and σ_i. Hereafter we employ $n_R = 3$ and $n_i = 2.5$.

Betatron Injection scheme

Optical parameters at the injection point and the emittance of the ring, as well as the injected beam are given in Table 10.3. The required injection

Table 10.3: Beam parameters for the betatron injection.

Parameter	HER	LER	unit
α_R	-7.93	-13.36	
β_R	100	100	m
ε_R	4.6	3.2	nm
ε_i	4.77	12.78	nm
Δx	7.8	8.4	mm
$\Delta x'$	-0.62	-1.1	mrad

aperture of the ring a_{xR} as a function of the beta-function, β_R, of the injected beam is shown in Figure 10.3a. The effective thickness of the septum has been assumed to be 2.5 mm. Assuming the beta-function of the ring $\beta_R = 100$ m, for example, an optimum value of the beta-function of the injected beam that makes the injection aperture minimum is found to be $\beta_R = 15.3$ m and 28.7 m for HER and LER, respectively. Though the larger β_R than 100 m gives the smaller injection aperture, its gain is not so significant considering an adverse effect of the larger chromaticity and the necessary larger physical-aperture.

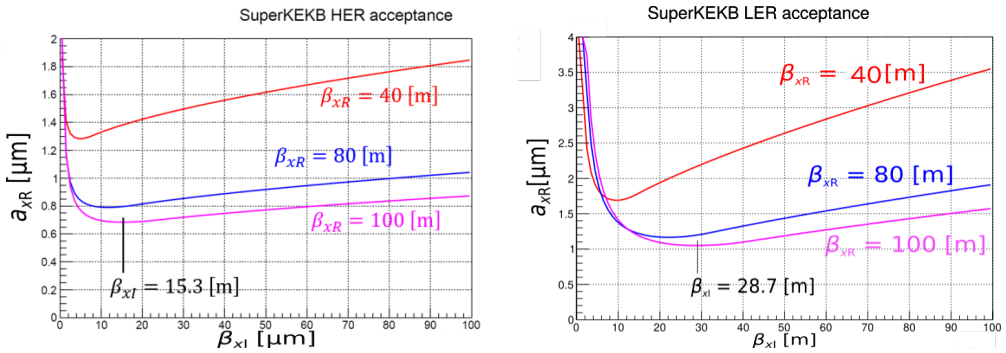

(a) HER (b) LER

Figure 10.3: Injection aperture in the case of betatron injection.

We have adopted $\beta_R = 100$ m as the design value. The orbit around the injection point is shown in Figure 10.4. Passing through a long slit opened at the one side the ring chamber, the injected beam enters the ring. The beam position and angle at the injection point, which is defined as the exit of the septum magnet, is given in Table 10.3, where Δx and $\Delta x'$ are relative position and angle of the injected beam to the stored beam at the injection point.

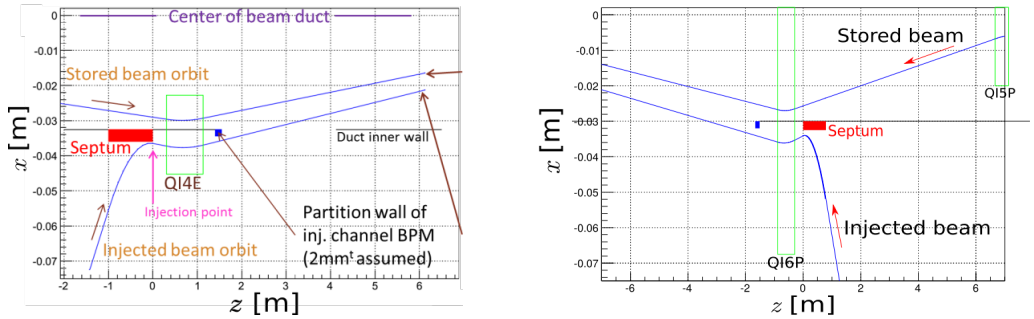

(a) HER (b) LER

Figure 10.4: Orbits of the injected beam for the betatron injection.

Synchrotron Injection scheme

The condition that the incoming beam is injected onto the closed orbit with the energy offset δ_i is given by

$$\eta\,\delta_i \quad = \Delta x \tag{10.13}$$

$$\eta'\delta_i \quad = \Delta x' \ , \tag{10.14}$$

where η and η' are dispersion and its slope in the ring at the injection point, while Δx and $\Delta x'$ are relative position and angle of the injected beam to the stored beam, *i.e.,* closed orbit bump by injection kickers. Above conditions ensures that no coherent betatron-motion is induced. However, an incoherent betatron oscillation is induced if beta functions of the injected beam does not match that of the ring. A condition to minimize the beta-mismatch is

$$\beta_i = \beta_R, \quad \alpha_i = \alpha_R. \tag{10.15}$$

From Eqs. (10.12)(10.13)(10.15), the energy offset of injected beams required for the synchrotron injections is given by

$$\delta_i = \eta^{-1}\left(w_s + n_R\sqrt{\varepsilon_R\beta_R + (\eta\sigma_\varepsilon)^2} + n_i\sqrt{\varepsilon_i\beta_R}\right), \tag{10.16}$$

where, we assumed dispersion of the injected beam disappears at the injection point: $\eta_i = 0$. Figure 10.5 shows the energy-offset as a function of the dispersion, where the curves correspond to different value of beta functions at the injection point. Here we have assumed $w_s = 2.5$ mm, $\varepsilon_R = 4.6$ nm, and $\varepsilon_i = 4.77$ nm. The maximum energy deviation of the injected beam, *i.e.*, required energy-acceptance, is given by

$$\varepsilon_{max} = \delta_i + n_\varepsilon\sigma_{\varepsilon i}, \tag{10.17}$$

where, $\sigma_{\varepsilon i}$ is the energy spread of the injected beam. Hereafter we employ $n_\varepsilon = 2.5$. Figure 10.6 shows the ε_{max} as a function of η for the case of $\beta_R = 20$ m. The required energy-acceptance is strongly dependent on the energy-spread of the injected beam. For the assumed energy-acceptance of

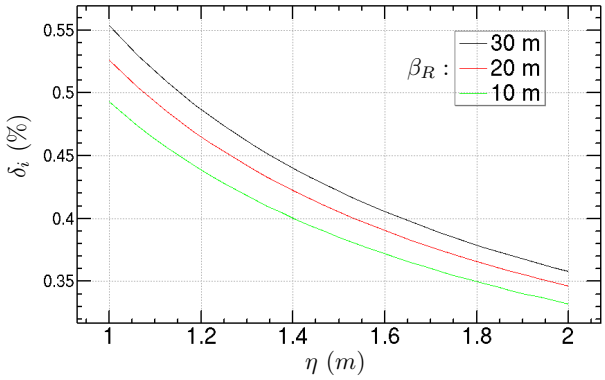

Figure 10.5: Dependence of the energy-offset on the dispersion at the injection point.

0.65 m, which is the design value of the main rings, parameters $(\varepsilon_{max}, |\eta|)$ of (0.1 %, 1.5 m) or (0.125 %, 2 m), for example, are required.

The beam parameters for the synchrotron injection scheme are shown in Table 10.4. Beam orbit in the synchrotron injection scheme is shown in Fig. 10.7. Because the effective septum thickness of the septum magnets used for the KEKB is $w_s = 4.0$ mm, it is unusable for the SuperKEKB injection system for both of LER and HER. It is thus necessary to reconstruct septum magnets nearest to the ring: one septum magnet in LER and two septa in HER.

10.2.2 Design of Septum Magnet

The effective thickness of 4 mm in the old septum magnet breaks down into the conductor with 1.5 mm thickness, two 0.5 mm-thick silicon steel sheet for magnetic shielding against the leakage field, and tiny spacings between them that amounts to 1.5 mm in total. In order to reduce effective thickness down to 2.5 mm, we use a conductor with thickness of 1.0 mm instead of 1.5 mm in the old system, and a single 0.5 mm-thick silicon steel for shielding. The larger tensile stress generated by the thinner conductor can be recovered by reducing the gap height to 8 mm from 11 mm. Utilizing a chamber made

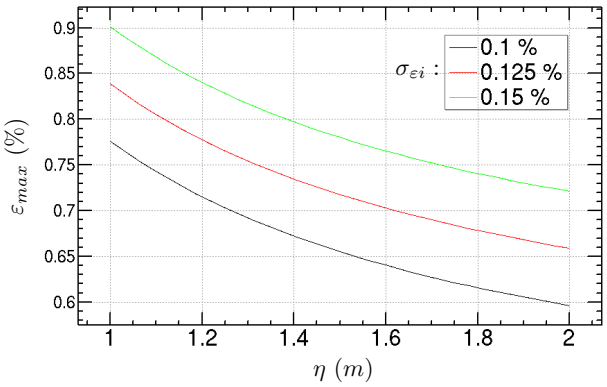

Figure 10.6: Energy acceptance as a function of the dispersion at the injection point for the case of β_R=20 m.

Table 10.4: Beam parameters for the synchrotron injection scheme.

Parameter		Value	unit
Beta-function of the ring	β_R	20	m
Beta-function of injected beam	β_i	20	m
Emittance of the ring	ε_R	4.6	nm
Emittance of the injected beam	ε_i	4.77	nm
Dispersion of the ring	η_R	-1.4	m
Energy spread of the stored beam	σ_ε	0.059	%
Energy spread of the injected beam	$\sigma_{\varepsilon i}$	0.1 †1	%
$(n_R, n_i, n_\varepsilon)$		(3.0, 2.5, 2.5)	
Effective septum-width	w_s	2.5	mm
Energy offset	δ_i	0.41	%
Orbit difference at injection	Δx	4.1	mm
Energy acceptance	ε_{max}	0.65	%

†1 Ref. [4] .

of iron for the ring, enough shield-effect can be obtained even for a single silicon-steel sheet. Considering the beam impedance, inner surface of the iron

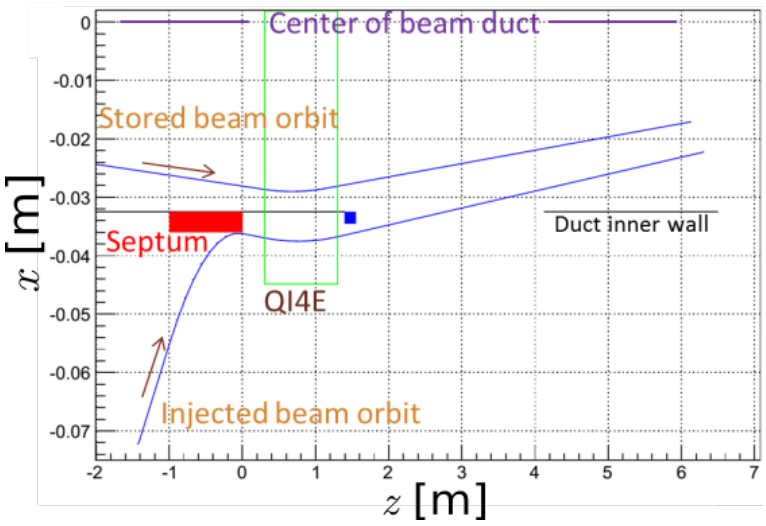

Figure 10.7: Orbits at the injection region in the case of synchrotron injection scheme.

chamber is plated with copper of 0.3 mm in thickness. A schematic view of the proposed design of the new septum magnet is shown in Fig. 10.8.

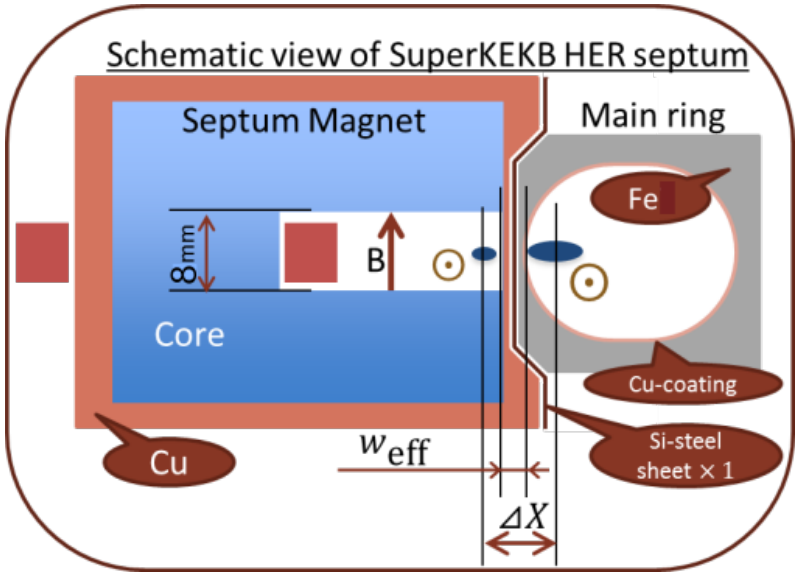

Figure 10.8: Cross-sectional view of the septum magnet in the design concept. The width of the Si-steel sheet is 0.5mm.

10.2.3 Field measurement of the prototype for the septum magnet

We have constructed a prototype for the septum magnet. Figure 10.9 shows the photos of the prototype magnet in the setup for the field measurement, where a mock-up beam pipe, which is made of ferromagnetic SUS430 stainless steel, was attached on the septum conductor. In the measurement, a

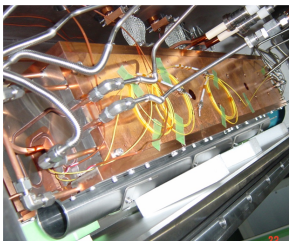

Figure 10.9: Photos of a prototype of the septum magnet. A mockup of the beam pipe made of ferromagnetic SUS430 stainless steel is attached on the septum conductor for the field measurement.

field mapping was performed in the median plane using a 10-turn pickup coil that has an area of 20×0.5 mm^2. The result is summarized in Fig. 10.10. The vertical axes are magnetic flux density and the horizontal axes indicate the transverse position in the line perpendicular to the beam direction in the median plane, where the origin of x is on the inner (gap-side) surface of the septum conductor, and the region of $x < -1$ mm corresponds to the outside of the septum while the $x > 0$ represents inside of the gap. The left inset of the figure shows the field in the gap as well as the leakage field in outside of the septum conductor, while the right inset shows the enlarged data for the outside of the septum, exhibiting the dependence of the leakage field on the shield materials and their combinations. A single shield of the Si-steel sheet of 0.5 mm thickness is not sufficient to suppress the leakage nor is the SUS430 chamber. Coexistence of the SUS430 chamber and Si-steel sheet are necessary for the leakage field to be suppressed less than a few Gauss. In the field

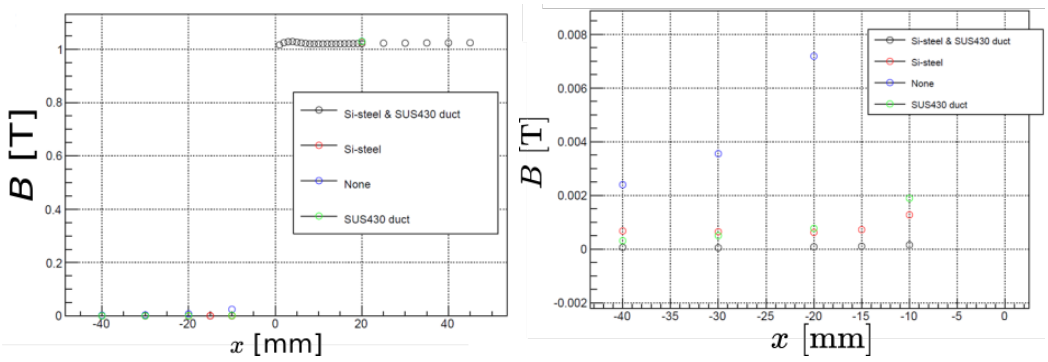

Figure 10.10: Results of the magnetic field measurement along the lateral position. Data-set for various shield conditions are shown; SUS430 duct only (green open-circle); No shielding (blue open-circle); Si-steel sheet only (red open-circle); and both of Si-steel sheet and SUS430 duct (black open-circle).

measurement we found a non-uniformity in the gap field of the septum magnet, which might affect the quality of the incoming beam. We have checked the effect using the field data by a beam tracking simulation. Traversing the gap field, the change of the bend angle is obtained as a function of the relative transverse position to the beam center. In Fig. 10.11 plotted is the angle difference from that of the beam-center. The horizontal axis is the relative position to the beam center at the entrance of the septum, in unit of the beam size. The thick (red) line represents the result of a fit to a straight line, slope of which manifests the existence of a quadrupole component. Subtracting the quadrupole component, a higher-order field component still remains, as shown in Fig. 10.12. The quadrupole component can be compensated by adjusting the quadrupoles in the upstream transport line, while the effect of higher-order component cannot be recovered. The maximum angle difference is 1.2 μrad, which is negligibly small compared with the natural divergence angle of the injected beam of $n_i\sqrt{\varepsilon_i/\beta_i} = 24.4$ μrad, thus the rate of unrecoverable distortion is only about 5%. Similarly evaluation of high-order position deviation with respect to the beam center shows that it is negligibly

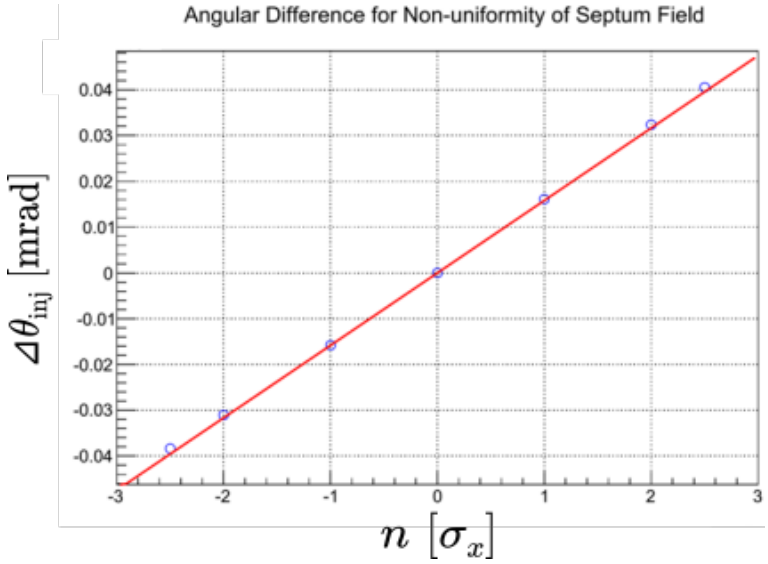

Figure 10.11: Angle difference from that of the beam-center. The horizontal axis is the relative position to the beam center at the entrance of the septum, in unit of the beam size. Thick (red) line represents the result of a least-square fit to a straight line.

small compared to the angle deviations.

10.2.4 Remedies for the vacuum degradation of MR due to outgas from septum magnets

In KEKB operation, it has been pointed out that the vacuum of the beam ducts of main ring in the vicinity of septum magnets abruptly degraded at a certain beam current[2]. This phenomenon had frequently interrupted the beam accumulation after the beam-abort. Outgassing from the core of the septum magnets has been strongly doubted as a possible source, considering a situation that the vacuum baking of the septum core had been insufficient; the vacuum of the the septum chamber had been rather poor and it had connected to the ring chamber through openings like a beam channel for the incoming beam as well as the spacings between bellows finger of the ring chamber.

Several mitigation for the issue are adopted.

- Enforce the baking system of the septum chamber.

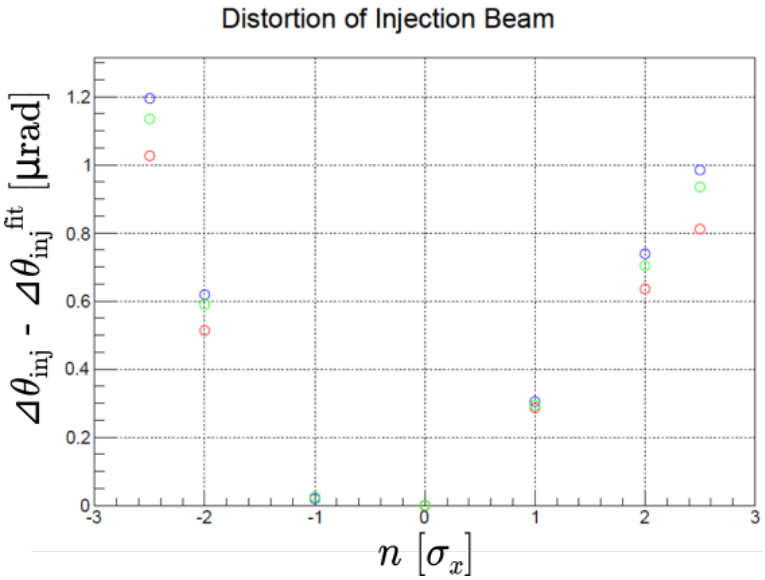

Figure 10.12: Residual in the angle difference after subtracting the first order component. Three data set corresponding to different shim type are shown; (blue) open circles for shim height of 0.08 mm and shim-width of 1.0 mm; (green) open circles for shim height of 0.1 mm and shim-width of 0.5 mm; (red) open circles for shim-height of 0.06 mm and shim-width of 1.0 mm.

- The vacuum chamber of the ring that is installed inside the septum chamber is replaced with a new one that has no opening to the septum chamber except for the beam channel for the injected beam.
- To prevent the outgas flowing through the beam channel to the ring chamber, a differential pumping system is installed between the septum chamber and the ring chamber, by introducing a narrow beam channel between them: 8 $\text{mm}^H \times 12$ $\text{mm}^W \times 0.5$ m^L for LER, and 5 $\text{mm}^H \times 12$ $\text{mm}^W \times 0.5$ m^L for HER.

With these improvements vacuum of the ring chamber is estimated to be within 10^{-6} Pa even vacuum in the septum chamber get worse to 10^{-4} Pa.

10.2.5 Power supplies for septum magnets

Figure 10.13 shows the schematic diagram of septum power supplies for the injection septum of HER and LER. The same power supply is used for the injection- and extraction-septum magnet of the damping ring(DR). The main

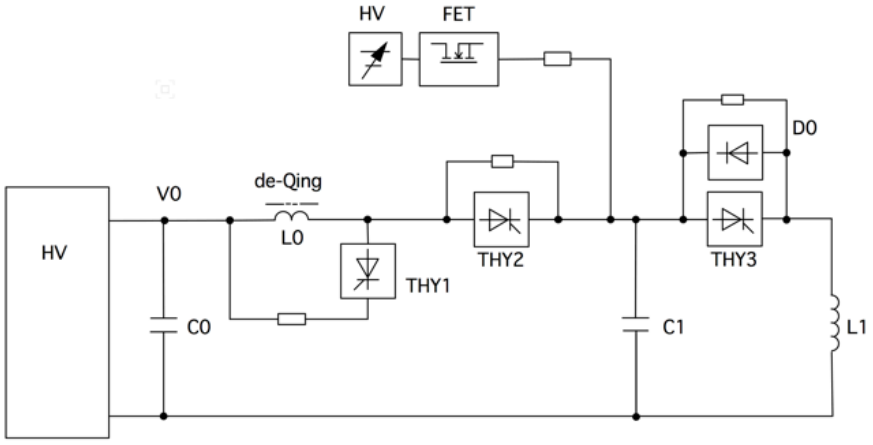

Figure 10.13: Schematic diagram of power supplies for the septum magnets.

capacitors (C1) are discharged by making the thyristors switches (THY3) turn on. The regenerative power is recharged to the main capacitors through diodes (D0) which are connected to the thyristors switches (THY3) in parallel. This gives the full sine pulse shape of about 250 μs. The leakage fields at the circulating beam are expected to be reduced in its slow component by using the full-sine pulse shape. Actual pulse shape is not perfectly symmetrical between positive and negative swing due to a resistive component of the main circuit. Figure 10.14 shows the current waveform at the magnet coil.

After the voltage of C1 is regenerated up to 86 % of the initial voltage, the main capacitors are re-charged up to the 99 % of the target voltage,

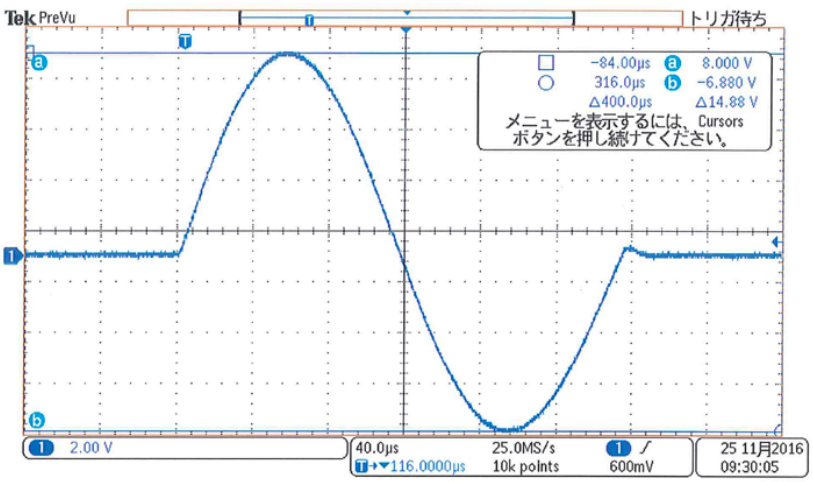

Figure 10.14: Current waveform for the DR injection septum.

which is determined by a de-Qing circuit, with a resonant charging through C0 and L0. The start timing of resonant charging is controlled by the thyristors switches (THY2). Finally, the power supply using the transistor dropper(FET) precisely controls the voltage at the main capacitor C1. The main parameters for these septum magnets are summarized in Table 10.5. The voltage stability of 0.01 % is required at any repetition rate. Figure 10.15 and Fig. 10.16 show the voltage stability at the start of operation and that after 1 hr, respectively.

Table 10.5: The main parameters of the septum magnets for the DR injection, DR extraction, HER and LER.

	DRinj	DRext	HER1,2	HER3,4	LER1	LER2	unit
Deflection angle	78.8	103	37.5	37.5	50	50	mrad
No. of magnets	1	1	2	2	1	1	
Aperture (h,v)	(70,24)	(70,30)	(44,9)	(44,11)	(44,9)	(44,11)	mm
Inductance†	5.77	4.7	9.6	7.6	7.6	6.0	μH
Charging voltage	1.2	1.8	1.44	1.58	1.29	1.43	kV
Peak current	7.0	11.4	5.5	7.6	5.4	7.4	kA
Stability	0.1	0.01	0.01	0.01	0.01	0.01	%

† at 3.3kHz

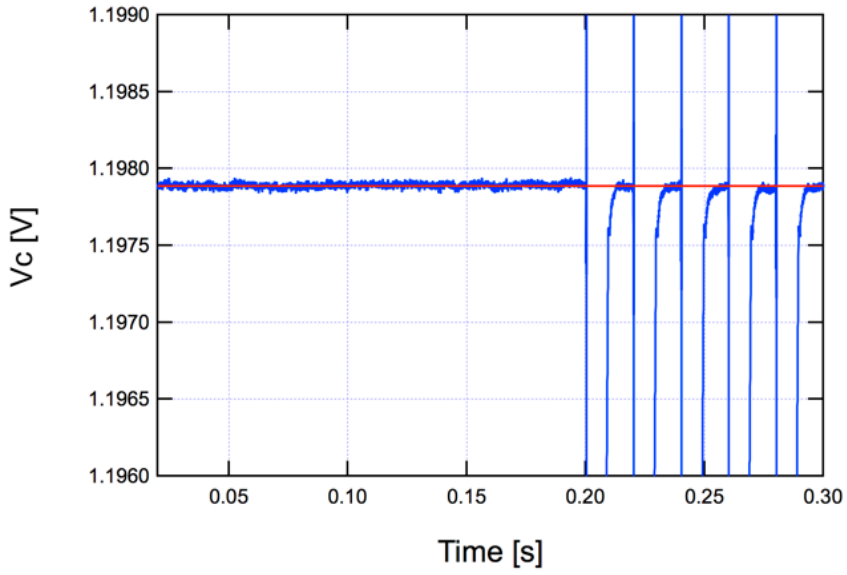

Figure 10.15: Voltage stability of the main capacitor of the power supply for the injection septum at the start of operation.

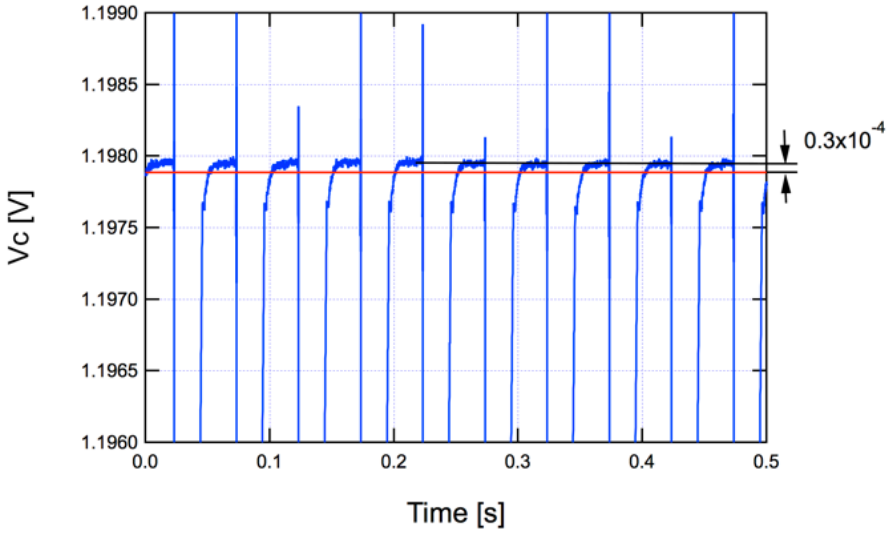

Figure 10.16: Voltage stability of the main capacitor of the power supply for the injection septum observed after 1 hr operation with a repetition frequency of 20 Hz.

Bibliography

[1] "KEKB Design Report",
http://www-acc.kek.jp/kekb/publication/KEKB_design_report/

[2] M. Kikuchi, *et al.*,"Beam-transport system of KEKB", Nucl. Instr. Meth. A 499 (2003) pp. 8-32

[3] T. Mori *et al.*, "Design Study of Beam Injection for SuperKEKB Main Ring", IPAC'12, New Orleans Luisiana, USA, May 2012, TUPPR089 (2012),
http://accelconf.web.cern.ch/AccelConf/IPAC2012/papers/tuppr089.pdf

[4] K. Furukawa *et al.*, "High-Intensity and Low-Emittance Upgrade of 7 GeV Injector Linac toward SuperKEKB", IPAC'13, Shanghai, China, TUPME010 (2013).